

High-Resolution Retinal Imaging of Cone-Rod Dystrophy

Jessica I. Wolfing, MS,^{1,2} Mina Chung, MD,^{1,3} Joseph Carroll, PhD,¹ Austin Roorda, PhD,⁴
David R. Williams, PhD^{1,2,3}

Purpose: This study examines a patient with cone-rod dystrophy using high-resolution adaptive optics retinal imaging. Conventional ophthalmoscopes provide limited resolution due to their inability to overcome the eye's optical aberrations. In contrast, adaptive optics ophthalmoscopes correct these aberrations to provide noninvasive high-resolution views of the living retina. To date, adaptive optics ophthalmoscopy has been used mainly to examine the normal retina. Here we use adaptive optics ophthalmoscopy to image cone-rod dystrophy in vivo and compare these results with standard clinical tests.

Design: Observational case report.

Methods: High-resolution retinal images of a patient with cone-rod dystrophy were obtained with the University of Rochester adaptive optics flood-illuminated ophthalmoscope and the adaptive optics scanning laser ophthalmoscope located at the University of Houston and compared with standard clinical tests, including fundus photography, Goldmann visual fields, fluorescein angiography, optical coherence tomography, electroretinography, and multifocal electroretinography.

Main Outcome Measures: Direct measurement of cone density and diameter and comparison of adaptive optics images with standard clinical imaging and functional tests.

Results: Adaptive optics images were acquired at multiple retinal locations throughout a clinically detected bull's-eye lesion. Within the atrophic regions, we observed large areas devoid of wave-guiding cones. In contrast, regions that appeared relatively spared by clinical examination contained a completely tiled cone mosaic. However, in these areas the cones were abnormally large, resulting in a 6.6-fold reduction from the normal peak cone density (patient peak density: 30 100 cones/mm², normal peak density: 199 200 cones/mm²). Multifocal electroretinography confirmed a 5.5-fold reduction in amplitude of the central peak (10.8 nanovolts/degree² vs. 59.8 nanovolts/degree²).

Conclusions: Adaptive optics ophthalmoscopy is a noninvasive technique to observe a patient's retinal pathology directly at a cellular level. It can provide a quantitative measurement of photoreceptor loss in retinal disease. *Ophthalmology* 2006;113:1014-1019 © 2006 by the American Academy of Ophthalmology.



Ophthalmoscopy is a fundamental element of the ophthalmologic examination because it allows the diagnosis of retinal disease by noninvasive observation of the retina through the natural optics of the eye. However, when pathologic changes have reached the level of resolution detectable by the ophthalmoscope, significant (and often irreversible) tissue damage usually has occurred. There has been considerable effort recently to develop retinal imaging modalities with increased resolution.¹⁻⁶ One obstacle is the

quality of the eye's optics. Correction of lower-order aberrations (defocus and astigmatism) coupled with scanning laser ophthalmoscopy or traditional fundus photography showed modest success in retinal imaging⁷ and visualizing individual cells in the retina.⁸⁻¹⁰ However, additional improvements in contrast and resolution can be obtained by using a wavefront sensor to measure the ocular aberrations and a deformable mirror to compensate for these aberrations.^{3,5} This adaptive optics ophthalmoscopy technique

Originally received: August 3, 2005.

Accepted: January 24, 2006.

Manuscript no. 2005-367.

¹ Center for Visual Science, University of Rochester, Rochester, New York.

² Institute of Optics, University of Rochester, Rochester, New York.

³ Department of Ophthalmology, University of Rochester, Rochester, New York.

⁴ College of Optometry, University of Houston, Houston, Texas.

Dr Carroll is currently at the Department of Ophthalmology, Medical College of Wisconsin, Milwaukee, Wisconsin, and Dr Roorda is currently at the School of Optometry, University of California, Berkeley, California.

Abstract presented in part at: Fall Vision Meeting, October 2004,

Rochester, New York, and Association for Research in Vision and Ophthalmology meeting, May 2005, Ft. Lauderdale, Florida.

Financial support from the National Institutes of Health, Bethesda, Maryland (grant nos.: EY01319, EY04367, EY07125, EY014375), is acknowledged. This work has been supported in part by the National Science Foundation Science and Technology Center for Adaptive Optics (Santa Cruz, California), managed by the University of California at Santa Cruz (cooperative agreement no.: AST-9876783).

The authors have no conflict of interest with regard to the material in the article.

Reprint requests to Jessica Wolfing, University of Rochester, Meliora Hall 274, Rochester, NY 14627.

provides a transverse resolution of $<2 \mu\text{m}$, which is necessary to image individual photoreceptors in the living retina routinely.^{3,5,11–14} It has been proposed that adaptive optics ophthalmoscopy could be used for early noninvasive detection and diagnosis of retinal pathology, but to date, most reports have involved only normal eyes (though see Carroll et al¹⁵ and Roorda¹⁶). Here, we use adaptive optics to examine the retina of a patient with cone-rod dystrophy (CRD).

Cone-rod dystrophy encompasses a heterogeneous group of retinal disorders defined electrophysiologically by a greater loss of cone than rod function.¹⁷ Histologic studies of CRD have shown regional photoreceptor loss, regional loss of the retinal pigment epithelium (RPE), and accumulation of lipofuscin.¹⁸ Genetically, autosomal recessive, autosomal dominant, and X-linked transmissions have been reported. The genotypic and phenotypic heterogeneity of CRD makes the study of cellular pathologic mechanisms a challenge. Here, adaptive optics ophthalmoscopy allows noninvasive direct observation of the retina of a patient with CRD at a microscopic resolution comparable to that of histology. To our knowledge, this is the first in-depth study of a progressive retinal degeneration utilizing adaptive optics ophthalmoscopy.

Materials and Methods

The research presented in this study was approved by the institutional review boards at the University of Rochester and the University of Houston, complied with the Health Insurance Portability and Accountability Act of 1996, and followed the tenets of the Declaration of Helsinki. All light exposures adhered to the maximum permissible exposure limits set by the American National Standards Institute standards.¹⁹ After the nature and possible consequences of the study were explained, written informed consent was obtained from a CRD patient.

A complete ophthalmic examination, including fundus photography, fluorescein angiography, Goldmann visual fields (VFs), and electroretinography, was performed. Optical coherence tomography measurements were obtained using Stratus optical coherence tomography (version 4.1 software, Zeiss, Dublin, CA). Multifocal electroretinograms were obtained using a DTL fiber electrode on a Veris machine (version 5.1 software, Electro-Diagnostic Imaging, Inc., Redwood City, CA) at the School of Optometry at the University of Houston. One hundred three hexagonal signal responses were measured over the central 30° .

Adaptive optics images of the right eye were obtained with both the University of Rochester's adaptive optics flood-illuminated ophthalmoscope and the adaptive optics scanning laser ophthalmoscope (AOSLO) previously located at the University of Houston; specifications of these devices and schematics have been published.^{3,5,13} The right eye was dilated and cyclopleged using phenylephrine hydrochloride (2.5%) and tropicamide (1%). The patient's head was aligned and stabilized with the use of a dental impression on a bite bar.

The University of Rochester's adaptive optics ophthalmoscope measured the monochromatic aberrations over a 6.8-mm-diameter pupil with a Shack-Hartmann wavefront sensor and then corrected them with a 97-channel deformable mirror (Xinetics, Devins, MA). The retina was then illuminated with a 4-millisecond flash (650-nm wavelength, 40-nm bandwidth) from a krypton arc lamp, and a retinal image was obtained with a 6-mm-diameter exit pupil.

The patient was instructed to fixate at a designated location on a target consisting of radial lines and concentric circles; the eccentricity and direction of fixation determined the retinal location imaged on each flash. Retinal images were summed using a Matlab (MathWorks, Natick, MA)-based image registration algorithm, and overlapping images were merged using Photoshop (Adobe Systems Inc., San Jose, CA).

The AOSLO used a Shack-Hartmann wavefront sensor with a 37-channel Xinetics deformable mirror to measure and compensate for the eye's optical aberrations over a 5.8-mm-diameter pupil. A spot from a laser diode (660-nm wavelength) was raster scanned across the retina, and the reflection was focused through a confocal pinhole and collected by a photomultiplier tube (Hamamatsu, Hamamatsu, Japan). Images were acquired at 30 frames per second for both the $3\times 3f$ field size and the $1.5\times 1.5f$ field size. Fixation was maintained by having the patient fixate at one corner of the scanning square. Custom Matlab programs were used to correct for image distortion caused by the sinusoidal scan pattern of the fast-scan mirror¹³ and to register and add individual frames. In Photoshop, overlapping images were used to create a high-magnification montage of the central macula, which can be placed at the correct location in the retina using features in the fundus photograph.

Cone diameters were measured using a freely available image-processing program (ImageJ, National Institutes of Health, Bethesda, MD). In each image at a given retinal location, 10 cones were selected randomly for measurement. An intensity profile was obtained through the center of each cone. The full width at half maximum of this profile was measured twice and averaged to give the diameter for each cone. GraphPad InStat (version 5.00, GraphPad Software, Inc., San Diego, CA) was used to determine statistical significance between cone diameters for normal subjects and the CRD patient.

Cone density estimates were determined by using a direct counting procedure; within the adaptive optics images, cones were identified manually at each retinal location using ImageJ. The coordinates of the cones were stored in a text array, and cone density was estimated by dividing the number of cones by the retinal area.

Results

A 26-year-old otherwise healthy woman presented with progressive loss of visual acuity since age 6 years. Family history was negative, suggesting autosomal recessive inheritance. Visual acuities were 20/70 (right eye) and 20/400 (left eye). Ophthalmoscopic examination revealed an annular zone of retinal pigment epithelial atrophy in the macula (bull's-eye macular lesion) starting at approximately 3° from fixation. Arteriolar attenuation, retinal striae, vitreous opacities, and peripheral atrophy with stippling of the RPE were present in both eyes. Goldmann VFs showed a ring scotoma with a 5° area of central sparing in the V4e isopter (right eye). Fluorescein angiography revealed transmission defects in the areas of RPE atrophy and hypofluorescence in areas of increased pigment. There was no evidence of choroidal masking. Figure 1 (available at <http://aojournal.org>) shows the results of clinical photography.

Optical coherence tomography demonstrated retinal thinning (Fig 2); central foveal thickness was $106\pm 5 \mu\text{m}$ (normal thickness: $168\pm 23 \mu\text{m}$; $P<0.01$).²⁰ The nerve fiber layer thickness in the papillomacular bundle was normal; the retinal thinning was attributable to layers in the outer retina.

Electroretinography showed a severe reduction in amplitude under cone-specific conditions and a moderate loss of amplitude under rod-specific conditions (data not shown). Multifocal electro-

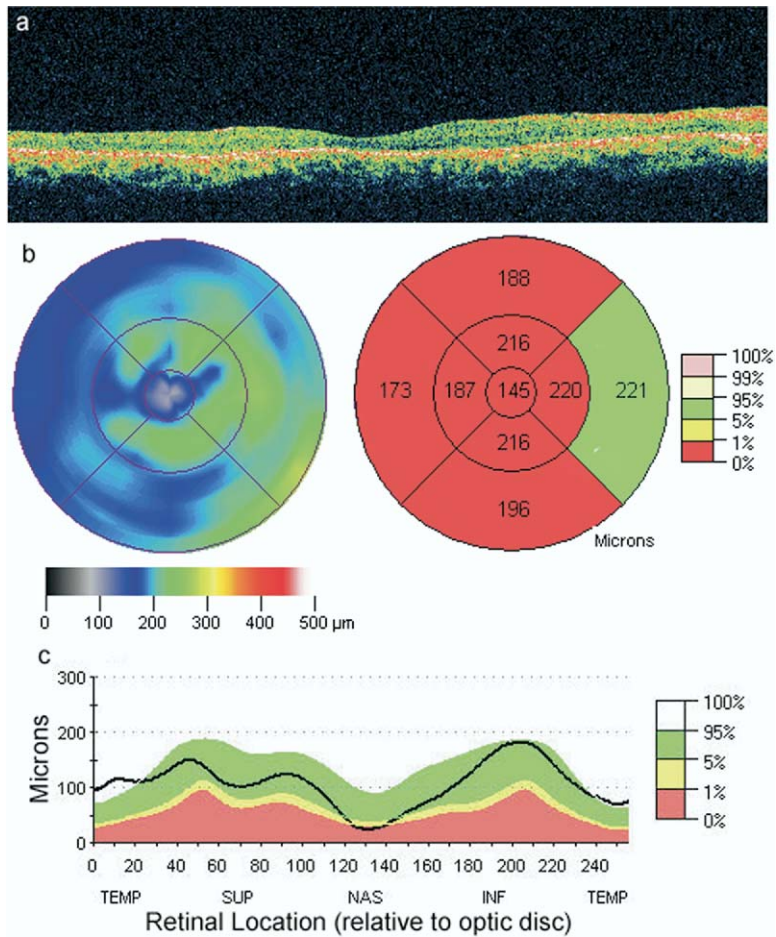


Figure 2. Optical coherence tomography results of the right eye. **a**, Seven-millimeter line scan through the fovea to the optic disc. The retina is thin at all locations along the scan. **b**, Left: retinal thickness map resulting from six 6-mm radial scans centered on the fovea. Right: macular thickness of each retinal section over the central 6 mm. The color code gives normative data for macular thickness; the patient's macula is thinner than normal ($P < 0.01$) in all areas except on the nasal side, where it is within the normal range ($0.05 < P < 0.95$). **c**, Retinal nerve fiber layer (RNFL) thickness obtained with a circular scan around the optic disc. The RNFL thickness is normal in the papillomacular bundle, suggesting that the thinning in the macula is attributable to deeper retinal layers. The RNFL thickness is lower than normal nasal to the optic disc. INF = inferior; NAS = nasal; SUP = superior; TEMP = temporal.

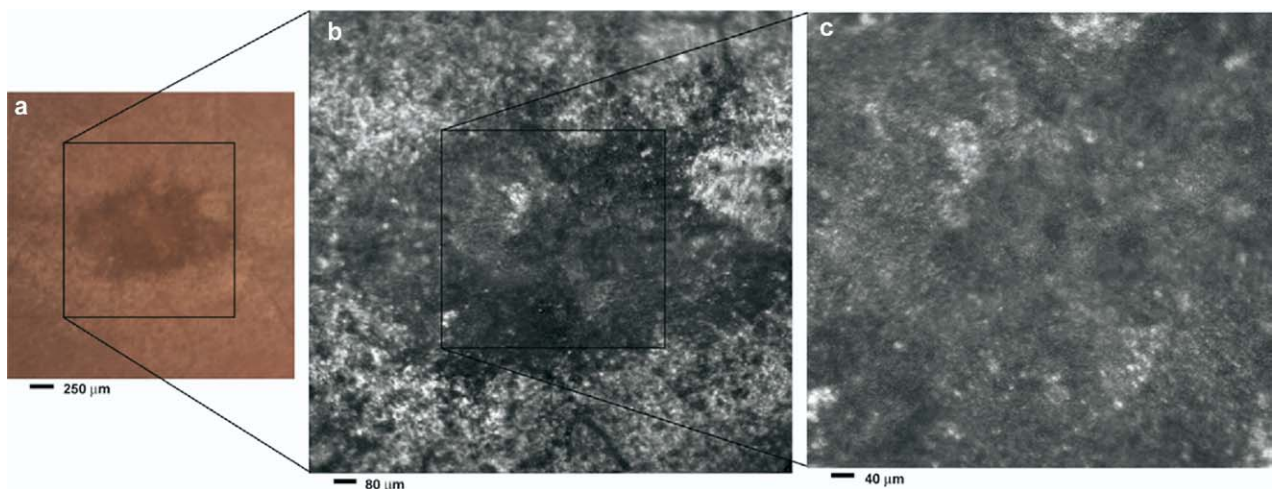


Figure 3. Adaptive optics scanning laser ophthalmoscope images at different magnifications with corresponding features on the fundus photograph (**a**). **b**, Six-degree montage from 3° adaptive optics images of the central macula of the cone-rod dystrophy patient's right eye. In addition to the features detected in the fundus photograph, detailed structures in the granular pattern of the retinal pigment epithelium in the atrophic bull's-eye lesion are observed. Within the central relatively spared region (box), photoreceptors are seen as gray dots. **c**, Three-degree montage from 1.5° images. The photoreceptors are visible in the central relatively spared area of the retina.

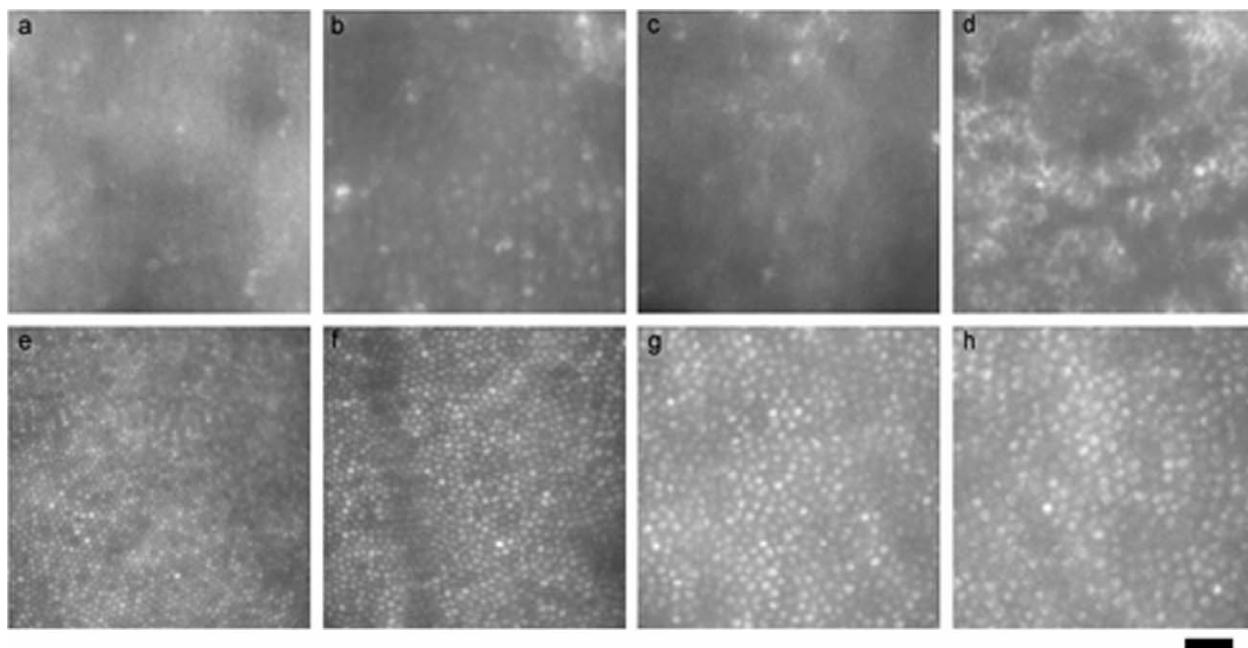


Figure 4. Top, Retinal images of the right eye of the cone-rod dystrophy (CRD) patient taken with the University of Rochester flood-illuminated adaptive optics ophthalmoscope at the center of the fovea and 1°, 2.5°, and 4° nasal to fixation, respectively. Bottom, Images of an age-matched normal subject at the same respective eccentricities temporal to fixation. A nearly continuous photoreceptor mosaic is observed in images corresponding to the relatively spared central retina of the CRD patient (a, b); however, the cones in these images are larger than cones observed in a normal subject's retinal image (e, f). c, d, The continuity of the photoreceptor mosaic breaks down in images of the bull's-eye lesion. Instead of a complete and continuous photoreceptor mosaic (g, h), dark patches of retina devoid of normal waveguiding cones and highly reflective patches of retinal scarring and atrophy are observed in the retinal lesion. Scale bar: 25 μm .

retinography showed diffuse reduction of cone function, consistent with previous reports²¹ (Fig 1c [available at <http://aaojournal.org>]). The central peak signal was 10.8 nanovolts/degree² (5.5 times less than normal [59.8 nanovolts/degree²]; $P < 0.01$).²¹

A 6° montage of the patient's central retina was obtained with the AOSLO (Fig 3). Individual cones in the central macula and detailed features in the bull's-eye lesion were observed and aligned with corresponding structures in the fundus photograph. Normally, cones are seen as bright spots; photoreceptors act as waveguides—light is coupled into and funneled through the photoreceptor, where it is reflected (presumably by the RPE) and guided out of the photoreceptor toward the center of the pupil.⁸ In the center of the bull's-eye lesion, which appeared relatively spared using conventional ophthalmoscopy, photoreceptors are seen as dots (Fig 3b). In the atrophic lesion, bright areas show the granular pattern of the RPE in addition to some remaining photoreceptors. The real-time view of the fundus during sequential movie frames confirmed that the patient maintained excellent fixation with the central fovea.

Using the Rochester adaptive optics ophthalmoscope, adaptive optics retinal images of the CRD patient were compared with those of an age-matched normal subject (Fig 4). In the center of the bull's-eye lesion, adaptive optics revealed a nearly continuous cone photoreceptor mosaic. Within 1.25° of the fovea, the cones were larger than normal ($P < 0.0001$, Mann-Whitney test), and cone density was decreased (Fig 5). At the foveal center, the patient's cone density was 30 100 cones/mm² (normal average, 199 200 cones/mm²).²² From 2.5° to 4°, the area corresponding to the atrophic bull's-eye lesion, patches devoid of normal waveguiding cones were interspersed with highly reflective areas showing the granularity of the RPE.

Discussion

To our knowledge, this is the first report to demonstrate pathologic findings in CRD using adaptive optics ophthalmoscopy and to compare these results with standard clinical and functional tests. The reduction in cone density observed in the adaptive optics images is a direct measure of retinal pathology in CRD. This measurement represents an upper limit on cone density for the patient; a liberal standard for counting was used, and densities were measured in areas of adaptive optics images where full mosaics were observed. Cone photoreceptor functional loss measured by multifocal electroretinography corresponded with the individual photoreceptor loss observed in adaptive optics images; multifocal electroretinography detected a 5.5-fold reduction in amplitude at the central peak, and adaptive optics images showed a 4.9-fold reduction in the photoreceptor density integrated over the central 1.25° region. The agreement found between the multifocal electroretinography amplitude and density results suggests that, for this CRD patient, the multifocal electroretinography amplitude is an estimate of the number of remaining photoreceptors. In this case, each remaining cone contributes a signal approximately equivalent to the amplitude a single cone would contribute in a normal subject's multifocal electroretinography summed response. However, given the cones' increased diameters (and increased areas available to absorb light), it is unlikely that all of the remaining photoreceptors are functioning normally.

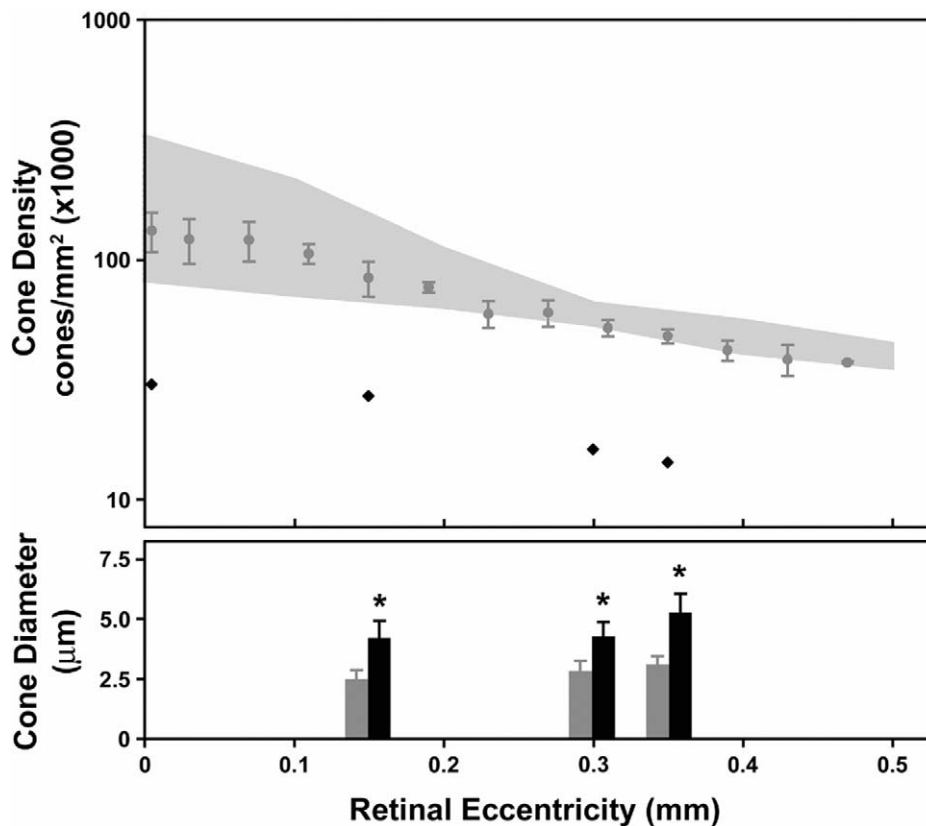


Figure 5. Cone density and cone diameter versus retinal eccentricity in normal subjects compared with the cone-rod dystrophy (CRD) patient. The patient's foveal cone density was reduced 85% from normal foveal cone density (30 100 cones/mm² vs. 199 200 cones/mm²). Measurements of cone density were made only in areas with a complete photoreceptor mosaic (central 1.25° for the cone-rod dystrophy patient). The light gray region is the normal range of cone densities measured using microscopy (Curcio CA, Sloan KR, Kalina RE, Hendrickson AE. Human photoreceptor topography. *J Comp Neurol* 1990;292:497–523). Dark gray bars show means and standard deviations of the normal cone diameter, and black bars show means and standard deviations of the cone diameter for the CRD patient. ●, mean and standard deviation of cone density of normal subjects measured from adaptive optics images using a direct counting procedure; ◆, cone density for the CRD patient. **P*<0.0001.

Currently, ophthalmologists rely primarily on conventional ophthalmoscopy and electroretinography results to make a diagnosis of photoreceptor degeneration. However, conventional ophthalmoscopes have limited resolution due to their inability to overcome the eye's optical aberrations, and full-field electroretinography measures photoreceptor function over a large field. Although this study involved only one patient with late-stage CRD, the utility of adaptive optics ophthalmoscopy is seen through the direct observation of retinal pathology and through the detection of photoreceptor degeneration. The AOSLO allowed a real-time view of the retina by which the retinal location was determined easily using features observed in fundus photography. Adaptive optics images from both systems revealed structures in the bull's-eye lesion and the relatively spared central macula that remain invisible using conventional ophthalmoscopy. Images of the bull's-eye lesion showed mottled, highly reflective microscopic areas of scarring and atrophy interspersed with dark patches of retina devoid of functioning waveguiding cones. The photoreceptor mosaic is visible in high-magnification images with the AOSLO, but individual photoreceptors were resolved more easily using the Rochester flood-illuminated adaptive optics oph-

thalmoscope. Further investigation is needed to interpret and quantify the features seen in these images; studies could include ultrahigh-resolution optical coherence tomography to detect local transverse photoreceptor loss,²³ autofluorescence imaging of the RPE,²⁴ and molecular genetic analyses to determine the disease-causing mutation in this patient. Additionally, longitudinal studies of disease progression or investigations of early-stage and presymptomatic CRD patients would help to determine the mechanism underlying the increased cone diameter and decreased cone density observed in this study.

Future applications for adaptive optics ophthalmoscopy include monitoring disease progression and investigating early disease mechanisms in retinal diseases such as CRD. In addition, adaptive optics ophthalmoscopy could enable novel therapies, such as gene replacement therapy, to be targeted to retinal locations with the most preserved photoreceptor mosaic, thereby directly increasing the potential for success of these therapies.²⁵ Adaptive optics ophthalmoscopy also could provide a safe noninvasive technique to measure treatment efficacies of these same therapies at a cellular level by examining photoreceptor survival rates in

humans and in preclinical trials involving animal models of retinal disease.

References

1. Artal P, Navarro R. High-resolution imaging of the living human fovea: measurement of the intercenter cone distance by speckle interferometry. *Opt Lett* 1989;14:1098–100.
2. Marcos S, Navarro R, Artal P. Coherent imaging of the cone mosaic in the living human eye. *J Opt Soc Am A Opt Image Sci Vis* 1996;13:897–905.
3. Liang J, Williams DR, Miller DT. Supernormal vision and high-resolution retinal imaging through adaptive optics. *J Opt Soc Am A Opt Image Sci Vis* 1997;14:2884–92.
4. Drexler W, Morgner U, Kartner FX, et al. In vivo ultrahigh-resolution optical coherence tomography. *Opt Lett* 1999;24:1221–3.
5. Hofer H, Chen L, Yoon GY, et al. Improvement in retinal image quality with dynamic correction of the eye's aberrations. *Opt Express* [serial online] 2001;8:631–43. Available at: <http://www.opticsexpress.org/abstract.cfm?URI=OPEX-8-11-631>. Accessed May 21, 2001.
6. Fernandez EJ, Iglesias I, Artal P. Closed-loop adaptive optics in the human eye. *Opt Lett* 2001;26:746–8.
7. Dreher AW, Bille JF, Weinreb RN. Active optical depth resolution improvement of the laser tomographic scanner. *Appl Opt* 1989;28:804–8.
8. Miller DT, Williams DR, Morris GM, Liang J. Images of cone photoreceptors in the living human eye. *Vision Res* 1996;36:1067–79.
9. Roorda A, Campbell MCW. *Vision Science and Its Applications*. 1997 Technical Digest Series. Vol. 1. Washington: Optical Society of America; 1997:90–3.
10. Wade AR, Fitzke FW. In vivo imaging of the human cone-photoreceptor mosaic using a confocal laser scanning ophthalmoscope. *Lasers Light Ophthalmol* 1998;8:129–36.
11. Roorda A, Williams DR. The arrangement of the three cone classes in the living human eye. *Nature* 1999;397:520–2.
12. Roorda A, Williams DR. Optical fiber properties of individual human cones. *J Vis* [serial online] 2002;2:404–12. Available at: <http://journalofvision.org/2/5/4/>. Accessed September 17, 2002.
13. Roorda A, Romero-Borja F, Donnelly WJ III, et al. Adaptive optics scanning laser ophthalmoscopy. *Opt Express* [serial online] 2002;10:405–12. Available at <http://www.opticsexpress.org/abstract.cfm?URI=OPEX-10-9-405>. Accessed May 6, 2002.
14. Pallikaris A, Williams DR, Hofer H. The reflectance of single cones in the living human eye. *Invest Ophthalmol Vis Sci* 2003;44:4580–92.
15. Carroll J, Neitz M, Hofer H, et al. Functional photoreceptor loss revealed with adaptive optics: an alternate cause of color blindness. *Proc Natl Acad Sci U S A* 2004;101:8461–6.
16. Roorda A. Adaptive optics ophthalmoscopy. *J Refract Surg* 2000;16:S602–7.
17. Berson EL, Gouras P, Gunkel RD. Progressive cone-rod degeneration. *Arch Ophthalmol* 1968;80:68–76.
18. Rabb MF, Tso MOM, Fishman GA. Cone-rod dystrophy: a clinical and histopathologic report. *Ophthalmology* 1986;93:1443–51.
19. American National Standard for Safe Use of Lasers. ANSI Z136.1-2000. Orlando: Laser Institute of America; 2000.
20. Wong ACM, Chan CWN, Hui SP. Relationship of gender, body mass index, and axial length with central retinal thickness using optical coherence tomography. *Eye* 2005;19:292–7.
21. Kretschmann U, Seeliger M, Ruether K, et al. Spatial cone activity distribution in diseases of the posterior pole determined by multifocal electroretinography. *Vision Res* 1998;38:3817–28.
22. Curcio CA, Sloan KR, Kalina RE, Hendrickson AE. Human photoreceptor topography. *J Comp Neurol* 1990;292:497–523.
23. Ergun E, Hermann B, Wirtitsch M, et al. Assessment of central visual function in Stargardt's disease/fundus flavimaculatus with ultrahigh-resolution optical coherence tomography. *Invest Ophthalmol Vis Sci* 2005;46:310–6.
24. von Ruckmann A, Fitzke FW, Bird AC. Distribution of fundus autofluorescence with a scanning laser ophthalmoscope. *Br J Ophthalmol* 1995;79:407–12.
25. Jacobson SG, Aleman TS, Cideciyan AV, et al. Identifying photoreceptors in blind eyes caused by RPE65 mutations: prerequisite for human gene therapy success. *Proc Natl Acad Sci U S A* 2005;102:6177–82.

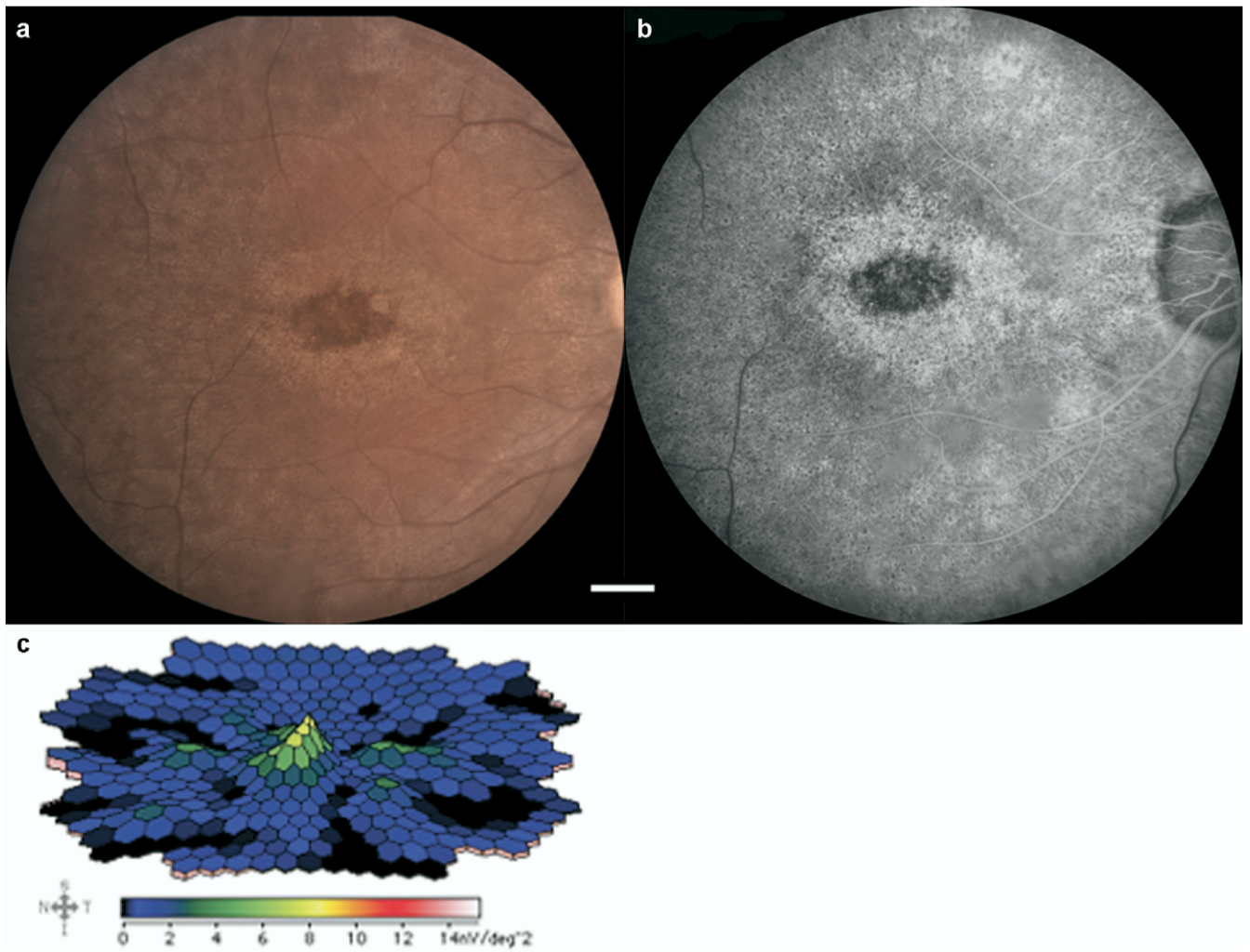


Figure 1. Fundus photograph (a) and fluorescein angiogram (FA) at 19 seconds (b) of the right eye of a patient with cone-rod dystrophy. The bull's-eye retinal atrophy begins at 3° eccentricity. The FA demonstrates an absence of choroidal masking and transmission defect in the atrophic bull's-eye lesion. Stippled hypofluorescent spots correspond to areas of pigment. Scale bar: 1 mm. c, Multifocal electroretinogram of the right eye, showing diffuse reduction in amplitude at all retinal locations. The central peak signal was 5.5 times less than normal ($P < 0.01$).